Characterization of Laser Deposited Ti-6Al-4V to Nb Gradient Alloys

Clincy Cheung

Senior Project Report

June 2015

Advisor:

Dr. Trevor Harding

Materials Engineering Department

California Polytechnic State University, San Luis Obispo

Approval Page

Project Title: Characterization of Laser Deposited Ti-6Al-4V to Nb Gradient Alloys

Author: Clincy Cheung

Date Submitted: June 5, 2015

CAL POLY STATE UNIVERSITY
Materials Engineering Department

Since this project is a result of a class assignment, it has been graded and accepted as fulfillment of the course requirements. Acceptance does not imply technical accuracy or reliability. Any use of information in this report is done at the risk of the user. These risks may include catastrophic failure of the device or infringement of patent or copyright laws. The students and staff of Cal Poly State University, San Luis Obispo cannot be held liable for any misuse of the project.

Dr. Trevor Harding
Project Advisor

_____
Signature

Dr. Katherine Chen
Department Chair

_____
Signature

Acknowledgements

- I would like to thank my advisor, **Dr. Trevor Harding**, for his patience throughout this school year. I suddenly, and almost haphazardly, wanted to pursue a project while still at JPL, but nonetheless you were more than happy to take me on as one of your senior project students. I appreciated all your advice, guidance, and humor throughout the process. Despite the challenges during the year, I would do this all again (although some parts differently!).
- Thank you to **Doug Hofmann**, **Scott Roberts**, and **Richard Otis** for providing me this opportunity to take some of your research samples and giving me the chance to experiment with something I have never even heard of. It was a worthwhile experience learning about this new technology and its science.
- Thank you to **Bryan McEnerney** and **Pete Dillon** for providing guidance throughout the project and your continued investment in me to succeed in my college and future career.
- Thank you to **Dr. Katherine Chen** for your knowledge and expertise in XRD, and insights into science and careers past college.
- To **Dr. Dan Walsh** for your expertise in metallurgy and being an amazing person to talk to about life experience and for your humor.
- To **Max Rosenberg** from the Aerospace Engineering department for your assistance putting together the MATLAB graphs. My data would not have looked vibrant as it does now without your help.
- To **Tyler Dinslage** for his advice and expertise on polishing. Without your suggestions, I would have taken much longer to get consistent mirror finishes!
- To the **MATE Department** for providing the wonderful lab space and resources for learning and experimentation.
- To **my parents**, who, despite being busy frequently, always find the time to talk and let me know that they are always behind me regardless of my choices in life. I love you both.

Abstract

An alloy was fabricated with Ti-6Al-4V and Nb powder using laser deposition (LD) to form a compositional gradient. The gradient was deposited, starting with Ti-6Al-4V powder, onto a forged Ti-6Al-4V substrate in an Argon environment. Niobium (Nb) composition increased by 4-at.% with each layer deposited until the composition reached 100-at.% Nb. This process yielded steep thermal gradients and affected the microstructure and mechanical properties across the compositional gradient. To observe the microstructural changes in the alloy, an etched gradient was viewed with optical microscopy at 1000x, where the grain structure was observed to be an acicular α phase at 100-at.% Ti-6Al-4V. As the at.% of Nb increased, the amount of β-Ti increased, the grain size decreased and the porosity increased. The 100-at.% Nb layers also exhibited porosity between layers. XRD scans of the LD Ti-6Al-4V indicated much less β-Ti present compared to the forged substrate. A peak shift in BCC with increasing Nb represented a gradual transition from β-Ti to Nb. A decrease in HCP peak intensities and increase in BCC indicated the decreasing amount of α-Ti and increasing amount of Nb along the gradient, where at 55-60 at.%, α-Ti was observed to be negligible. Microhardness was also used to probe the uniformity within layers and the change in strength across layers. A large variance was present in the layers of 50-90 at.%, while a general decrease in hardness was observed with the addition of Nb.

KEYWORDS

Ti-6Al-4V, laser deposition, additive manufacturing, gradient alloys, microstructure, X-ray Diffraction, energy dispersive X-ray spectroscopy, microhardness

Table of Contents

List of Figures

List of Equations

Introduction

Additive manufacturing, or 3-D printing, as it is commonly known, is a process where a part can be fabricated without the need for tooling. For metals, a technique known as laser deposition (LD) is used to fabricate a near net-shape part. This technique is commonly used for high-temperature alloys such as Inconel, a high-temperature superalloy that involves a significant amount of energy and cost to manufacture. By using laser deposition, the part can be fabricated with detailing and tight tolerances using a computer-aided drafting (CAD) file, leaving out the need for expensive tooling. This minimizes the amount of waste heat typical in a casting manufacturing process, while greatly reducing lead times and overhead for manufacturing.

An instrument for laser deposition is equipped with a build head, with powder blower attachments and a laser. The laser scans along a surface with powder blowers depositing the material onto a metal substrate, generating a melt pool with the metal powder, and solidifying a part one layer at a time. Figure 1 depicts a laser deposition instrument fabricating an alloy.

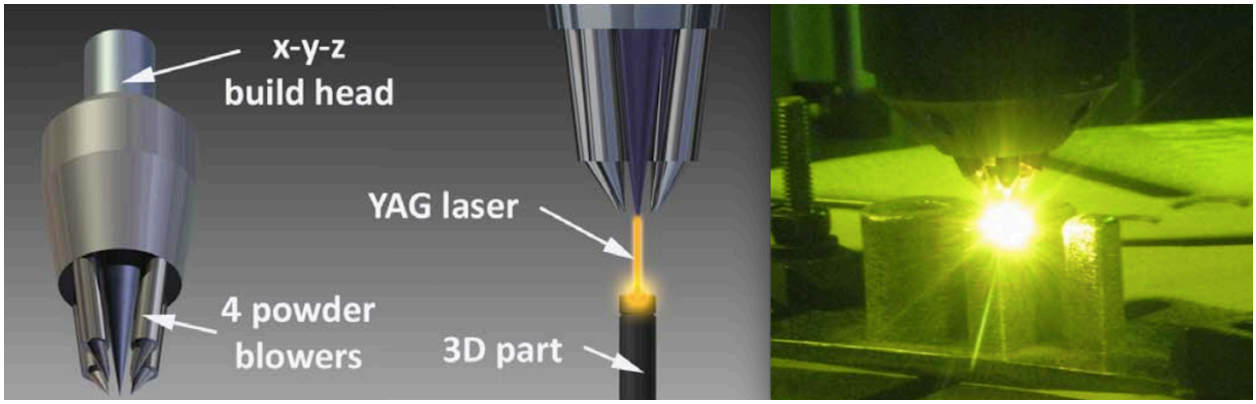

Figure 1: a.) An illustration of a laser deposition instrument depicting a part being built up one layer at a time; b.) actual image of an alloy being laser deposited.[1]

Gradient Alloys

A new class of materials known as gradient alloys has been developed using laser deposition. By implementing multiple powder blowers into a laser deposition system, the composition of a material can shift, layer-by-layer, along the distance of the alloy by switching the composition of the powdered metal during deposition. The purpose of this is to optimize the performance of an alloy for certain applications. An example of this would be a mount for a mirror on a spacecraft, where the mount is normally made out of Invar, an alloy with a low

coefficient of thermal expansion. By using laser deposition to fabricate a gradient alloy, 304L stainless steel can be used as the material for the base of the mount. As a result, this would reduce the amount of Invar needed, save cost, and replace and strengthen portions with stainless steel where Invar is not necessary. The method also serves as an alternative to welding, which is normally susceptible to formation of brittle intermetallic phases, decreasing ductility in the weld area. With laser deposition, the composition can be tuned in each layer of deposition in order to avoid the formation of intermetallics, while ensuring consistent bonding between layers. Researchers at Jet Propulsion Laboratory have developed a rocket nozzle using Ti-6Al-4V and Niobium (Nb) as the system components (Figure 2). In this conceptual application, the rocket body is manufactured with Ti-6Al-4V to provide the strength for the structure of the rocket. The nozzle would gradually transition to a higher concentration of Nb, where the ignition of the fuel takes place. The refractory property from higher Nb content is aimed to maintain strength at elevated temperatures.

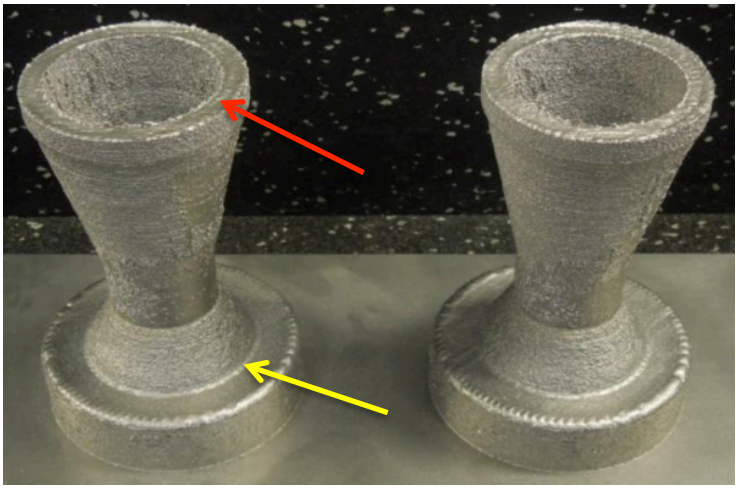

Figure 2: A Ti-6Al-4V to Nb gradient alloy in the form of a rocket nozzle prototype fabricated using laser deposition. The alloy gradually transitions from a Ti6Al4V alloy, indicated with a yellow arrow, to pure Niobium, indicated with a red arrow.

Factors of Laser Deposition

Although a quick manufacturing method, laser deposited alloys are not without constraints. Multiple factors can contribute to defects or undesired microstructures including, but not limited to: travel speed, spot size of the laser, and composition of the powder, all of which

can affect the strength and reliability of the alloy in service. To illustrate the effects of these factors, ~100% Ti-6Al-4V laser deposited alloys are used below.

Porosity

If insufficient power is used for the deposition of a metal, porosity may form as a result of insufficient heating. The amount of porosity in a deposited alloy varies inversely with the laser power since it determines the amount of energy inputted into the system to melt the components during deposition. A macrograph (Figure 2) of a Ti-6Al-4V alloy that has been deposited at a laser power of 900W indicates porosity. This is undesired since the areas with porosity will exhibit lower strength properties than the bulk material, leading to possible failure.

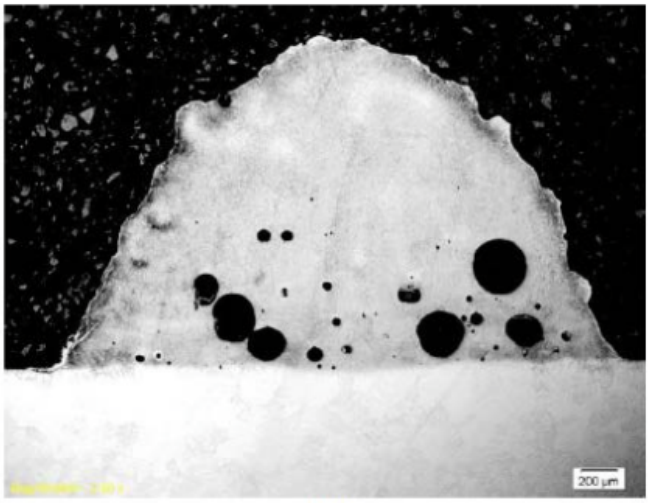

Figure 3: Porosity depicted in macrograph of Ti-6Al-4V with 1 wt.% Cu, laser deposited with a laser power of 900W. 1 wt.% Cu is negligible as T_m of Cu is much lower than the T_m of Ti.[2]

One concern in fabricating a Ti-6Al-4V to Nb gradient alloy is whether porosity forms within the structure. Since the amount of power needed to melt the powder increases significantly with the addition of Nb, a metal with a melting temperature of 2,469^{o}C, porosity could increase with increasing Nb if the power increase is not enough.

Effect of Cooling on Microstructure of Laser Deposited Titanium

The combination of travel speed, small spot size, and high power input generally yields a steep thermal gradient and rapid cooling from a melt pool. In a laser deposited structure of Ti-6.5Al-3.5Mo-1.5Zr-0.3Si, rapid cooling forms a fine-grained structure, where the melt pool

transforms from liquid into a Widmanstatten α. α-Ti nucleates preferentially on β-Ti grains and grow in multiple directions, or as large grains in a non-uniform manner (Figure 4). Particularly, large α-Ti boundaries that cross grain boundaries are detrimental to the properties of the structure, allowing the structure to be susceptible to cracking along the grain boundaries. Although the composition of Figure 4 is not Ti-6Al-4V, the amount of β-Ti between the layers of Widmanstatten α-Ti varies with the amount of β stabilizers present in the alloy.

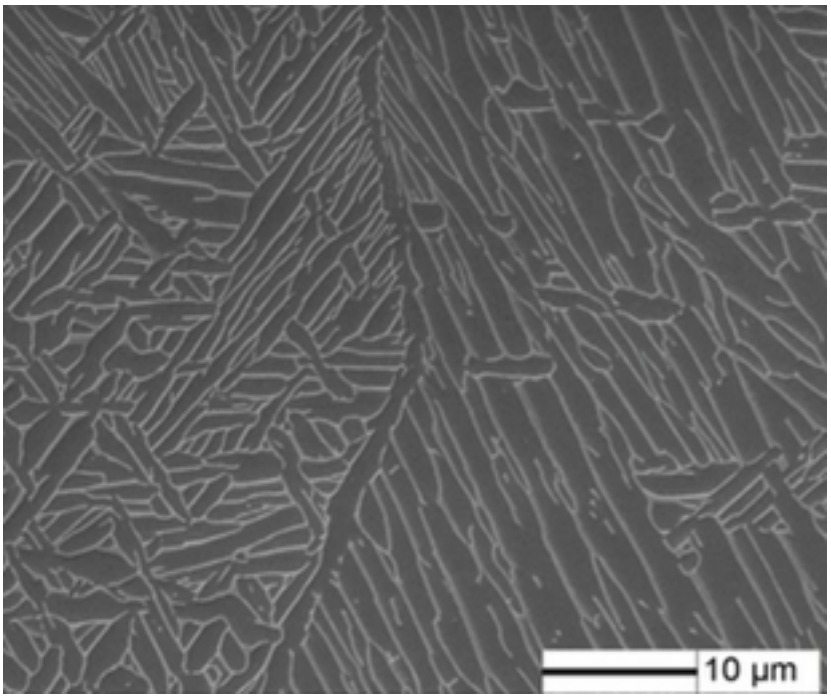

Figure 4: A laser deposited microstructure of Ti-6.5Al-3.5Mo-1.5Zr-0.3Si. The structure is more uniform on the left, while the right shows more single direction growth, reaching the dividing grain boundary.[3]

Problem Statement

Laser depositing Ti-6Al-4V and Nb to form a gradient alloy will yield different properties than pure Ti-6Al-4V with the gradual addition of Nb into each layer. Researchers at JPL predict that since the residence time of the laser on one portion of the alloy is short, the amount of mass transport or diffusion will be negligible.[1] However, a thermodynamic model done by JPL also predicts an annealed structure assuming that the laser releases residual heat throughout the alloy. As the microstructure is of importance to the strength and consistency of the alloy, this senior project study aims to observe the change in structure and strength of the

alloy across the laser-deposited gradient. The results will serve to evaluate the effectiveness of the gradient alloy in an aerospace application.

Experimental Procedure

The fabrication of the alloy was contracted out by NASA Jet Propulsion Laboratory and was fabricated by RPM & Associates in Rapid City, SD. Multiple techniques were employed to analyze the structure of the Ti-6Al-4V to Nb gradient alloy, including metallography, X-ray diffraction, scanning electron microscopy (SEM), energy-dispersive X-ray spectroscopy (EDS), and microhardness.

Processing Parameters

Two powder blowers were loaded, one with Ti-6Al-4V powder, and the other with pure Nb powder. Sixty-two layers were deposited on a Ti-6Al-4V substrate in an Argon environment. The first nineteen layers consisting of Ti-6Al-4V were deposited at a power of 910 W. The next twenty-four layers increased in concentration by 4 at.% Nb per layer, with power increasing by 9 W each layer. The last nineteen layers consisted of pure Niobium powder deposited at a max power of 1135 W. The hatch and contour travel speeds were both set at 12.7 mm/s with a spot size of 1.42 mm. The nominal deposited layer thickness is 500 μm. The posts were separated from the substrate using a band saw to isolate the posts with minimal substrate attached. The resulting shape of the substrate was square and each side of the cross section is 2.5 cm in length (Figure 5).

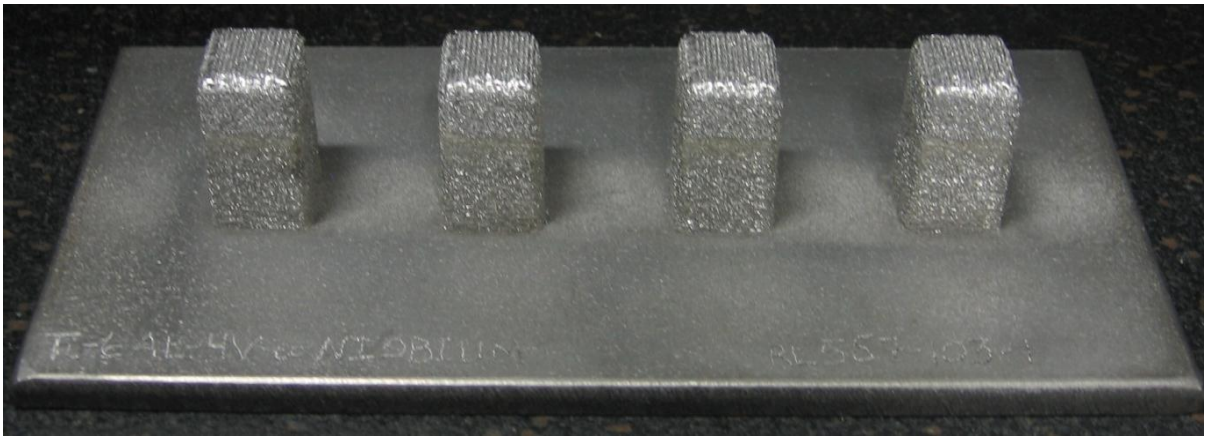

Figure 5: Posts of Ti-6Al-4V to Nb gradient alloys, laser deposited onto a titanium substrate.

Sample Preparation

A post of Ti-6Al-4V to Nb gradient alloy was separated from the substrate using a diamond saw at a rate of 200 rpm, while applying cutting fluid to prevent excess heating. After the post was removed, the post was sectioned into four lengthwise samples. The sample is assumed to have a small amount of curvature for each layer due to surface tension during the sintering process. Therefore, samples were cut lengthwise, dividing the cross-sectional area of the original sample into four, to ensure identical gradients across all samples in the same post. Both ends on two alloys were cut using the diamond saw at a rate of 200 rpm, leaving only the gradient portion with minimal pure alloys on the ends (Figure 6). Sample 1 was mounted in Bakelite, and sample 2 was mounted in acrylic.

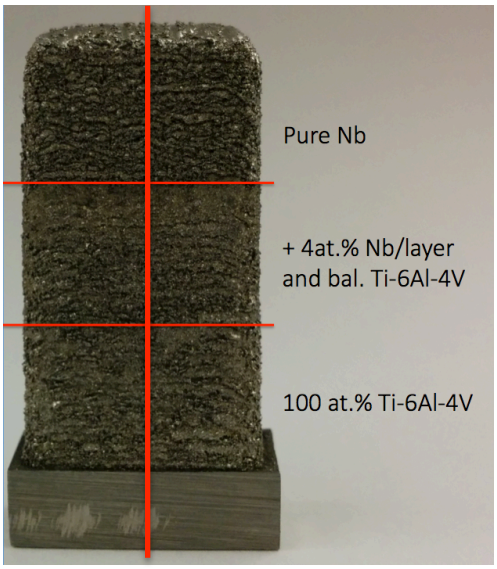

Figure 6: Gradient alloy sample with compositional markers. The red lines indicate where the alloy was cut.

Metallography

The sample 1 gradient was ground with 400 and 600-grit sandpaper. The samples were then taken through the 6 µm and 1 µm polishing wheels with diamond abrasive, until a mirror finish was achieved. An enhanced Kroll's Reagent, containing 50mL H_2O, 25mL HNO_3, and 5mL HF, was used to reveal the microstructure of the gradient.[4] The Niobium portion of the gradient was swabbed etched for 45 seconds, while the Ti-6Al-4V side was swabbed etched for six seconds. Samples were viewed under 100x and 1000x magnification to observe changes in microstructure.

Scanning Electron Microscopy/Energy Dispersive X-ray Spectroscopy

Scanning electron microscopy was used at a power of 30 kV at a magnification of 20x to view the gradient. Using the energy dispersive X-ray spectroscopy function on the microscope, points were taken across the gradient on sample 1 every 400 µm to determine the composition accuracy (Figure 7). Compositional measurements were graphed in comparison with the nominal composition and distance. Data from overlapping measurements between images were not used when the plot for composition was generated.

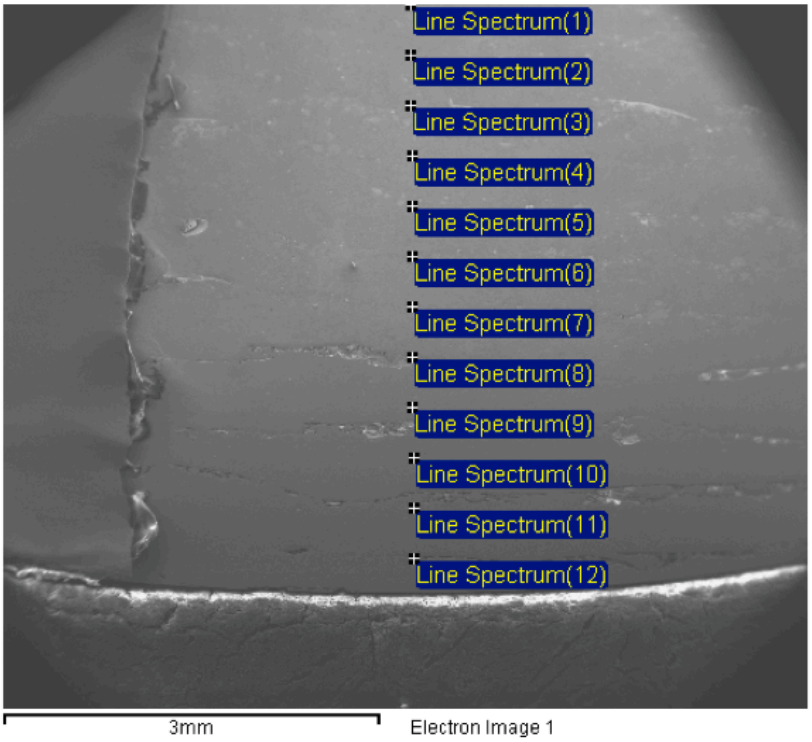

Figure 7: SEM image of spectra taken every 400 µm along one portion of gradient.

X-ray Diffraction (XRD)

An un-mounted sample was placed on a glass slide and scanned with X-ray Diffraction at a rate of 1^{o}/min at a voltage of 40 kV and current of 25 mA. The sample was scanned at the Nb end and subsequently shifted and scanned until the scan yielded peaks of Ti. The same was done for the Ti-6Al-4V end. The slide was marked to indicate pure Niobium and Ti-6Al-4V (Figure 8). Including the two points already marked, a total of nine evenly spaced points were marked on the slide to set a reference point for scan locations. Scans were taken after each point, starting

from the Nb end, to map the change in crystal structure across the gradient. MATLAB was used to produce a 3-D interpolated representation of all nine scans to show the shift in crystal structure and lattice.

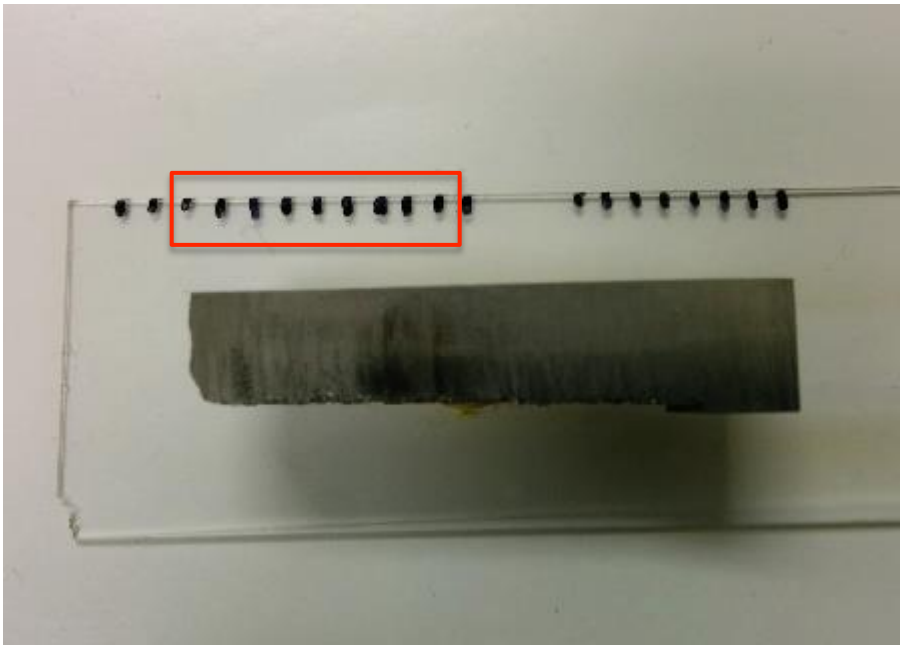

Figure 8: Unmounted sample of Ti-6Al-4V to Nb gradient alloy. In red, the marks used for XRD scan.

Microhardness

Hardness measurements were taken at 13 layers on sample 2, with five points laterally within each layer, for total of 65 points. Indentations were spaced such that measurements would not affect another, in accordance with ASTM E384.[5] A diagonal of each indentation was measured and the Vickers hardness was calculated using Eq. 1.

$$HV = 1.853 * 10^3 * \left(\frac{F}{d^2}\right) \qquad \textbf{(1)}$$

F = indentation load (in gf)
d = diagonal length (in µm)

Results and Discussion by Test Method

Microstructural Changes

There are general microstructural trends across the gradient, with a certain at.% of Nb for where each trend begins. As the composition increases, there is a decrease in grain size, increase in porosity density, and a decrease in the extent of columnar β-Ti growth after 30 at.% Nb. In the melting process, the Nb and Ti interdiffuse, but do not yield a complete solid solution. However, the slight interdiffusion between the two components significantly increased β-Ti across the gradient. Figure 9 showed a widmanstatten structure at 100 at.% Ti-6Al-4V, with small amounts of β-Ti in between the α-Ti laths. The α-Ti laths resulted from a high cooling rate from a steep thermal gradient until the sample dropped below the β transus. Small amounts of β-Ti formed first during cooling acting as nucleation sites for α-Ti to form into a widmanstatten structure. Since the laser continuously scanned, there was residual heat throughout the sample, which caused a slightly variable cooling rate and grain size as throughout the sample. This can observed between the left and right sides of Figure 9. Because of a composition with low β stabilizers and a high cooling rate, the volume fraction of β-Ti in this layer is the lowest in the gradient.

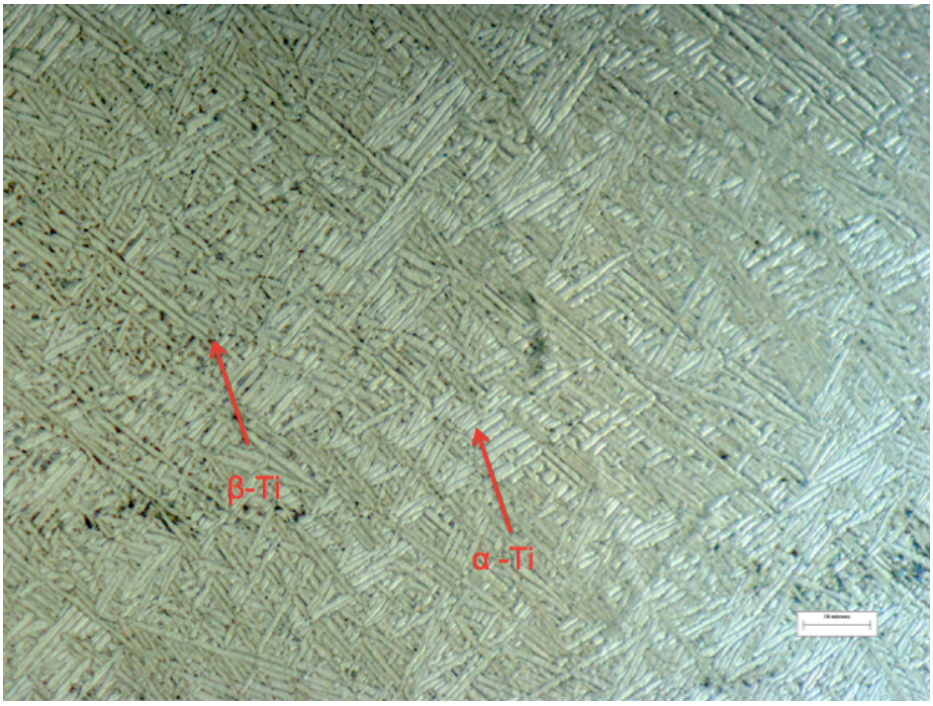

Figure 9: Deposited layer of 100 at.% Ti-6Al-4V.

Figure 10 shows a darkened structure with the introduction of 4 at.% Nb, which acted as a stabilizer for β-Ti within the structure. During the melting stage, the Nb solidified before the titanium alloy, due to a much higher melting temperature. Nucleation sites from solidified Nb and a higher concentration of β-stabilizers within the Ti-6Al-4V structure resulted in a finer widmanstatten structure, more commonly known as a basketweave structure.[6] Because of a higher β stabilizer amount, the volume fraction of β-Ti increased greatly in the structure as well as in between α-laths. As the concentration of Nb increases more across the gradient, the α-laths become smaller, while the amount β-Ti increases as well (Appendix B).

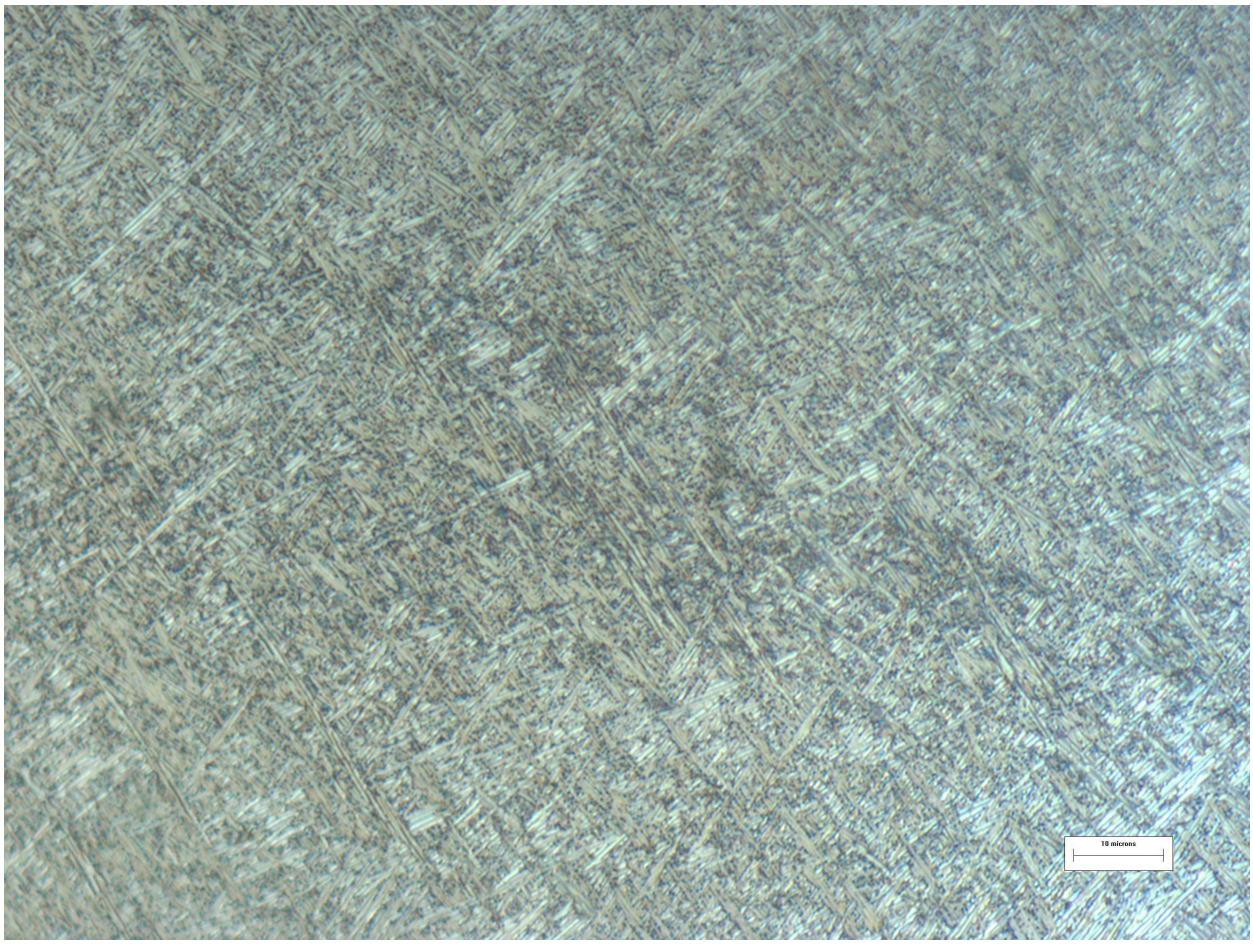

Figure 10: Deposited layer of 96 at.% Ti-6Al-4V, and 4 at.% Nb.

At around 30 at.% Nb (Figure 11), more β-Ti is present in the structure because of the increased Nb content and heat flow. β-Ti grains present in the structure solidified preferentially from the

effect of applied heat, forming columns of β-Ti along the heat gradient toward the top of the deposited layer. Nb solidification prior to β-Ti formation provided nucleation sites for β-Ti to nucleate epitaxially. As the Nb content increases, the extent of columnar growth decreases since there is less β-Ti available to nucleate epitaxially (Figure 12). At 100 at.% Nb (Figure 13), the layers of Nb exhibit a large amount of porosity within the layers. Because of insufficient heat during deposition, the layers of pure Nb are only partially bonded. Compositional segregation in Figure 11 and 12 is also observed in the structure because of differences in solidification time.

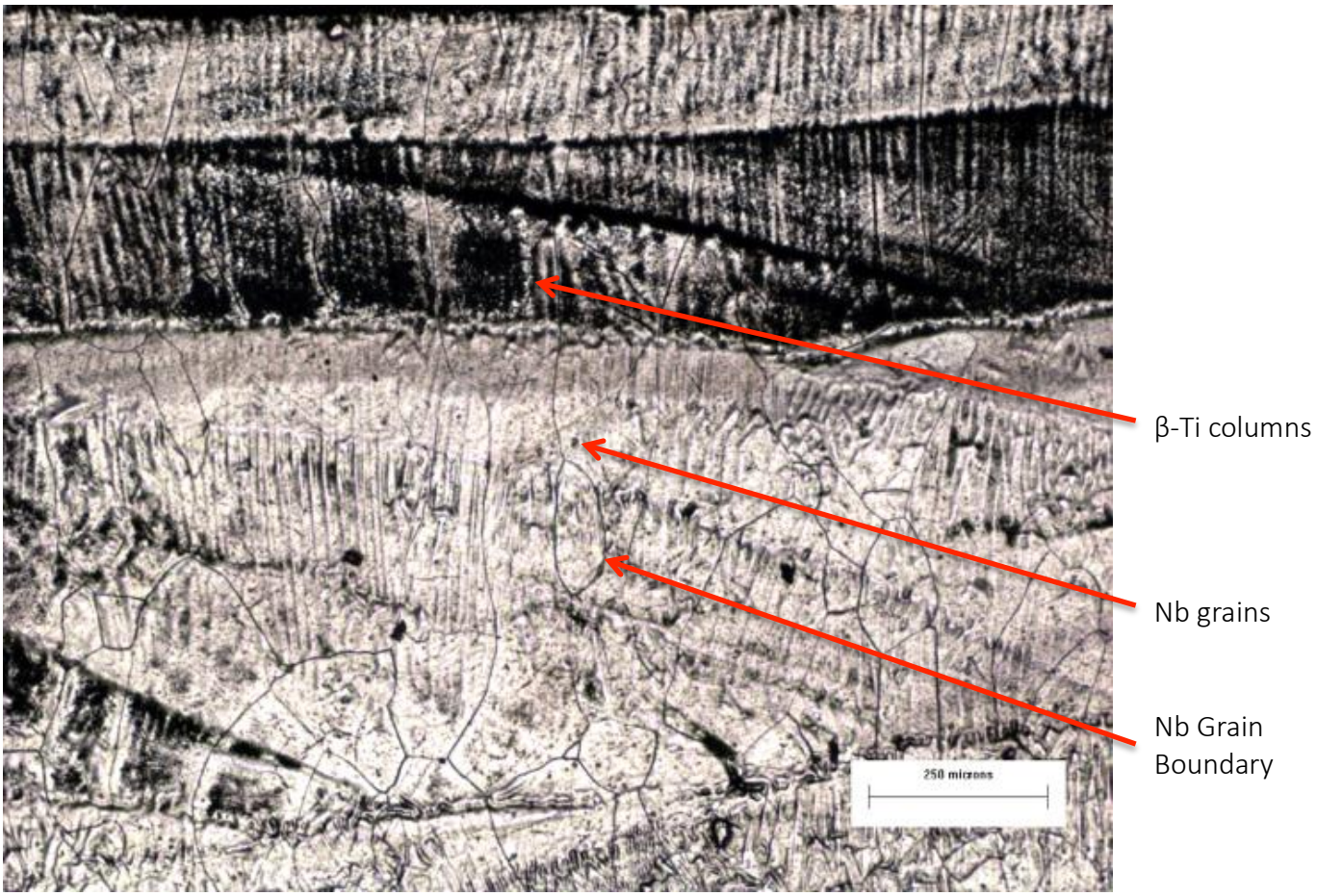

Figure 11: Deposited layer of approximately 30 at.% Nb, and bal. Ti-6Al-4V, marking columnar growth along deposited layer.

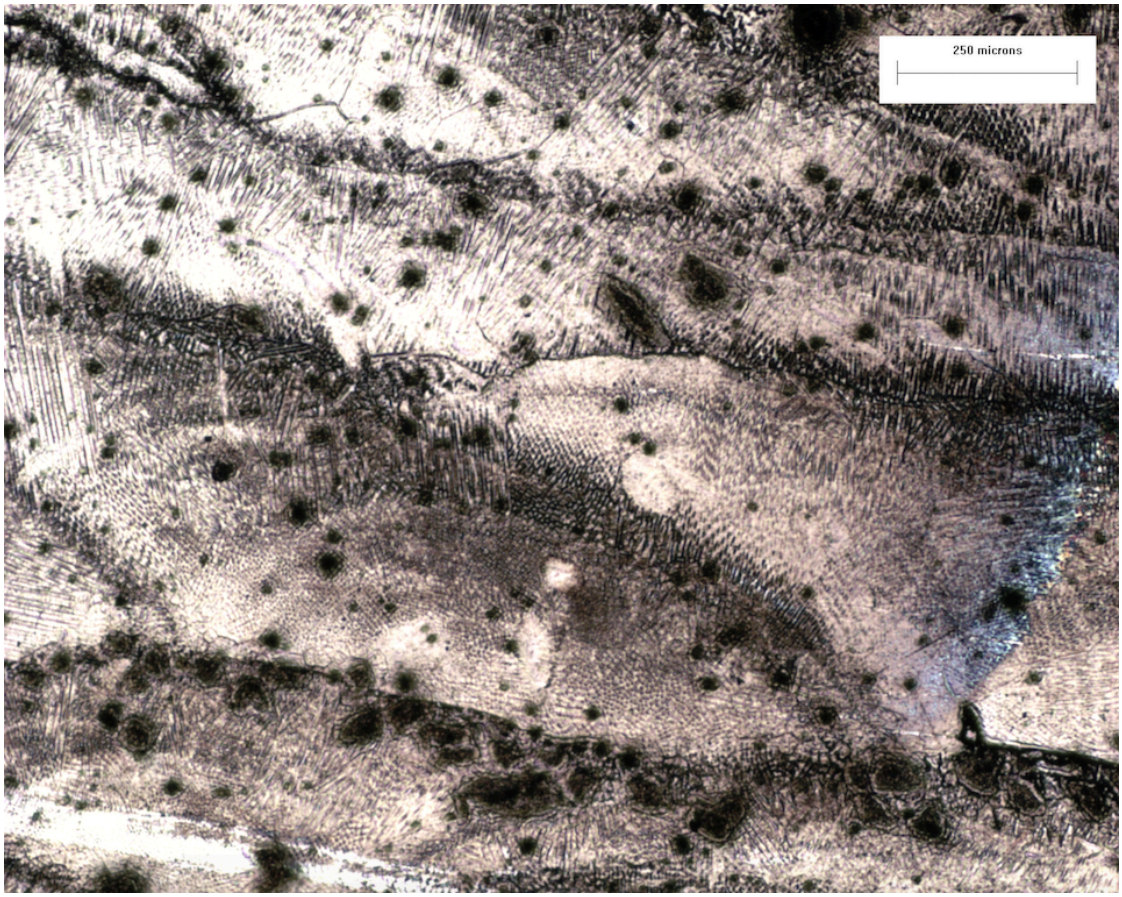

Figure 12: Deposited layer of approximately 50 at.% Nb, and bal. Ti-6Al-4V. Columnar growth is observed along the deposited layer. Dark circular regions are pores within the structure.

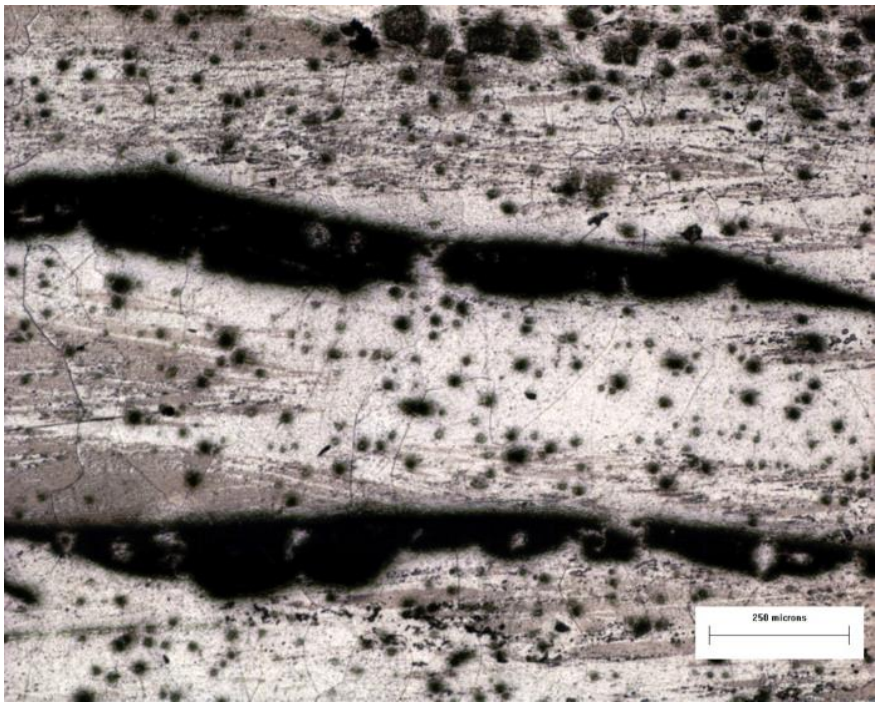

Figure 13: Deposited layer of 100 at.% Nb. Dark circular regions are pores within the structure. Large voids are also present in between layers.

Compositional Analysis

In a compositional analysis, the measured composition (Figure 14) of the Ti-6Al-4V and Nb components yielded a general decrease and increase, respectively. However, the Nb at.% reached 100 at.% at several millimeters shorter than the nominal composition, which assumed 4 at.% Nb for every 500 µm. In comparison, the gradient length of the actual composition was around 10.2 mm, where the nominal was targeted to be at 12.5 mm, likely shortened because of overmelting. When the laser power is too high for a particular layer, the layer beneath may melt and collapse slightly. Compositional segregation could also lead to inaccuracy since Nb solidifies first, leaving Ti to directionally grow as observed in the 50 at.% range.

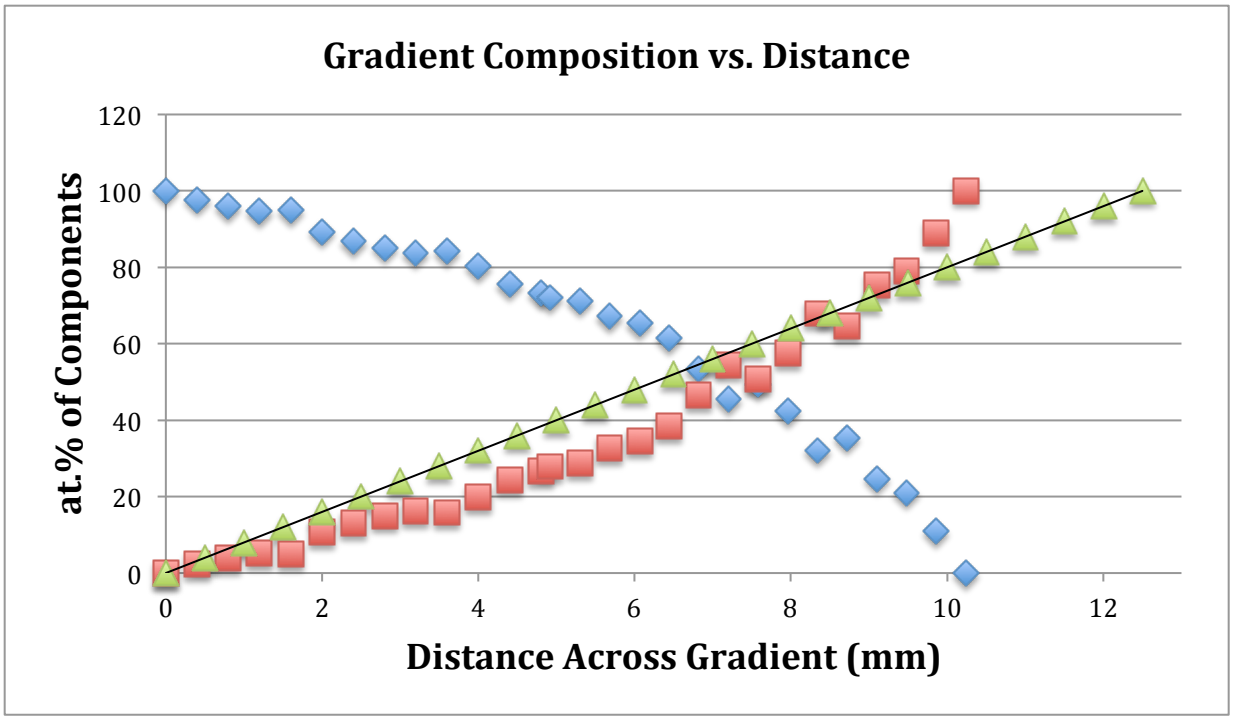

Figure 14: Measured composition using EDS on an SEM. The Ti-6Al-4V measurements are in blue while the Nb measurements are in red. The nominal composition is colored in green.

Crystal Structure and Phase Analysis

The XRD plot generated (Figure 15) illustrates the intensity as the composition changes from Ti-6Al-4V to Nb. There is a general decrease as expected when transitioning from the Nb with a BCC crystal structure to that of Ti-6Al-4V, consisting of a dominantly HCP structure.

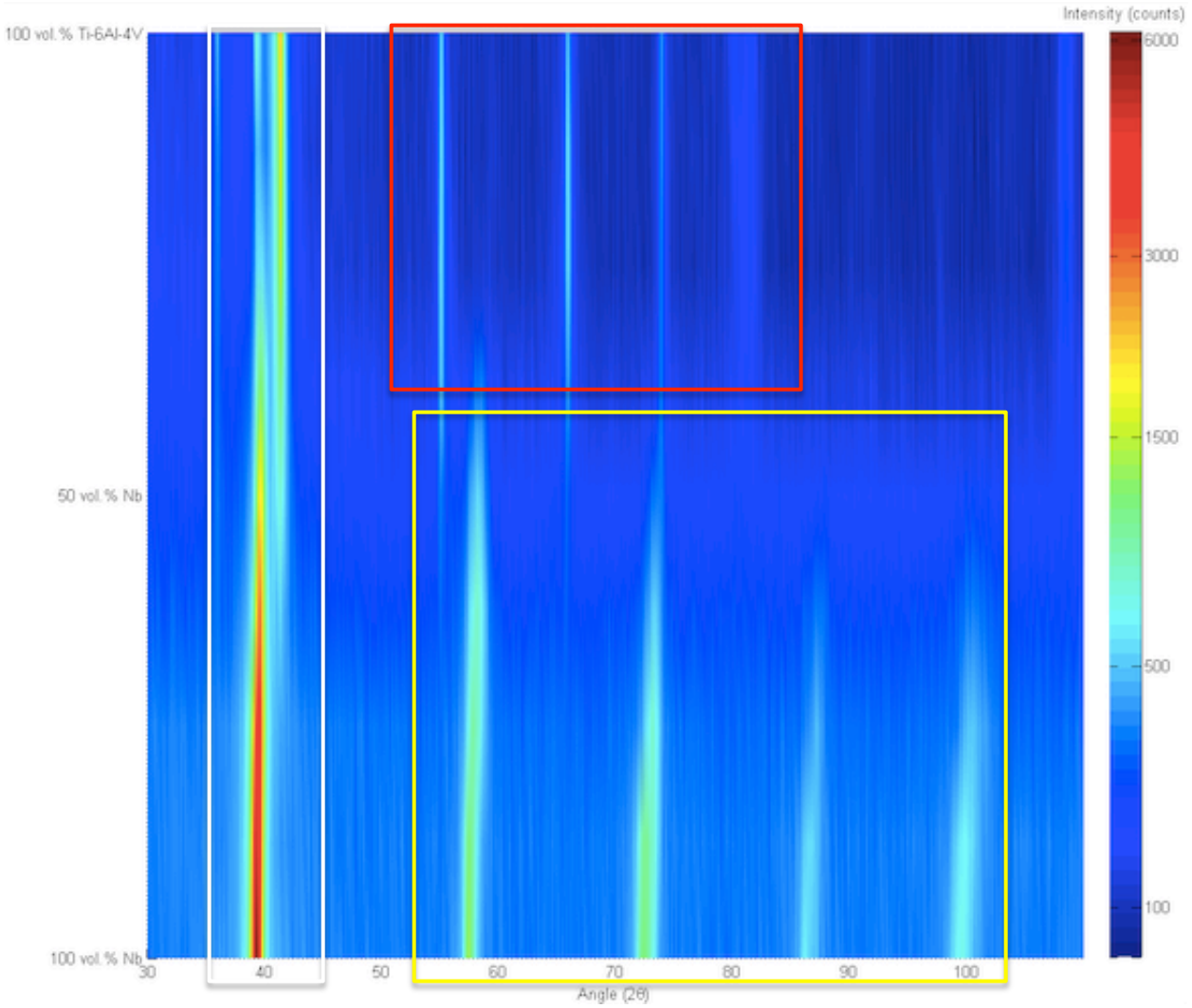

Figure 15: 2-D interpolated graph of all nine XRD scans plotted according to composition. Left white box highlights the broadest BCC on the left and HCP on the right. Red highlights the minor HCP peaks, while the yellow box highlights the minor BCC peaks.

The graph shows that the HCP crystal structure becomes negligible after 55-60 at.% Nb, at the main peak highlighted with a white box. This is supported by the microstructure present at 50 at.%, which shows little indication, if any, of α-Ti present in the microstructure. Referring to a binary phase diagram (Figure 16) for the major components, Ti and Nb, α-Ti does not form within the structure beyond approximately 38-40 at.% in a solid solution. However, since laser deposition involves complete melting but limited diffusion for each layer across the gradient, it can be assumed that there could be a small amount of un-solutionized α-Ti at high Nb content. This may not be observable using an optical microscope, but detectable on an XRD scan.

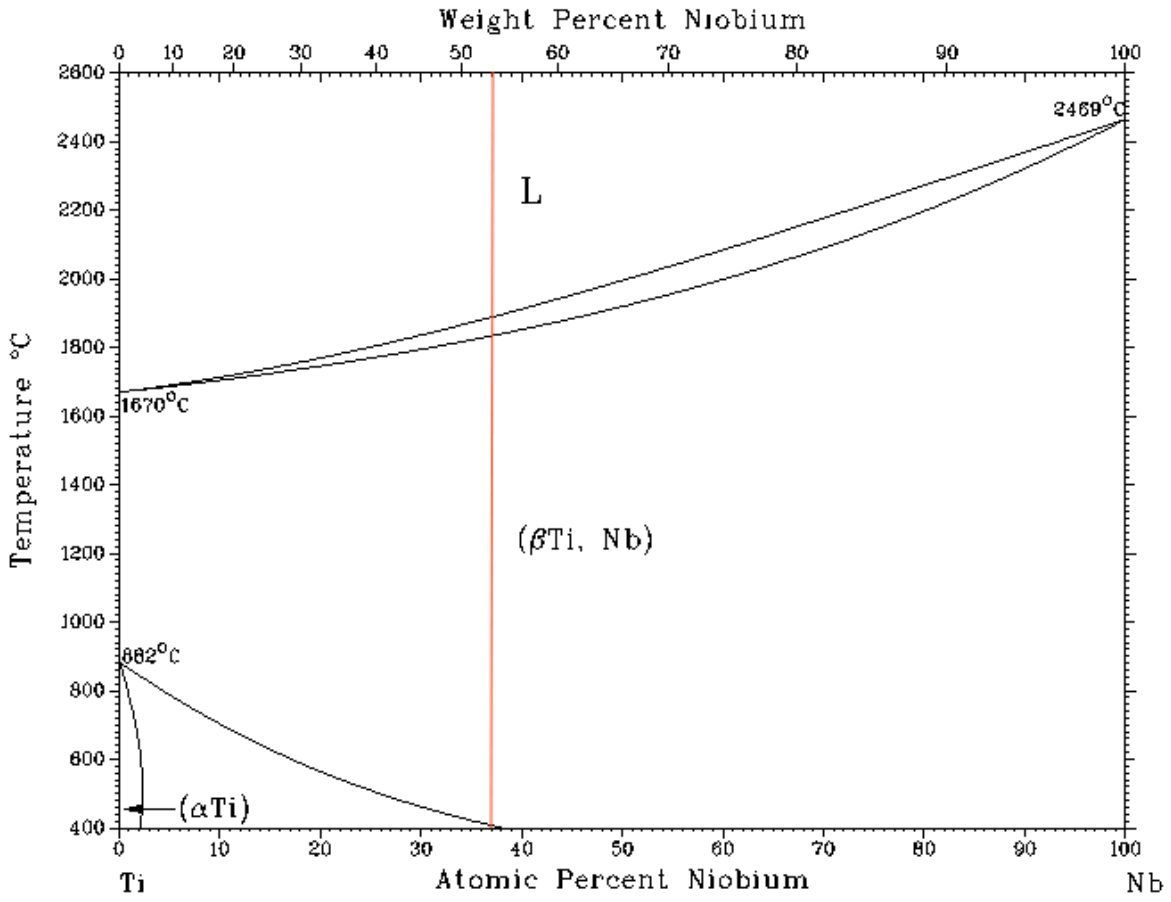

Figure 16: Ti-Nb binary phase diagram, with the red tie line indicating the point where only a BCC structure forms.[8]

The XRD scan is also based on distance with an assumed nominal composition at each scanned point, without knowing the actual composition at the scanned location. Depending on the location of the scan, the composition can be off when comparing the scan location with the EDS data in Figure 14. The scan also shows a slight shift in lattice in the BCC peaks, which is a result of slight alloying from diffusion and difference in lattice constants between β-Ti and Nb. The XRD scan also rejects the assertion from JPL's research that mass transport is kinetically negligible given the short residence of the laser, strong implying a mixture of components. If the alloy deposition were kinetically negligible, the scan would show HCP peaks along >90% of the distance of the scan. With increasing Nb, the lattice shift would also look sharper since individual scans would yield more resolved peaks of pure elements. Peaks within the yellow box on Figure 15 would be narrower indicating a more resolved overall scan, if the gradient were to be a simple mixture of Ti and Nb.

Microhardness

The gradient showed a general decrease in strength as the measurements were taken toward the Nb side (Figure 17). Acicular Ti, a more general term for the widmanstatten and basketweave structures in the pure Ti, registered the highest hardness value. With the addition of Nb, a soft and ductile metal, the hardness dropped within the area where the majority component is still Ti-6Al-4V. When the amount of Nb increases to occupy a majority of the structure, the columnar β-Ti, a stronger and less ductile phase of titanium strengthens the structure. However, the amount of variance also increased since the amount porosity increases. While taking a hardness measurement, it may be possible to indent an area with an unseen pore beneath, or take a measurement where columnar β-Ti and Nb can exist in the same layer. The two boxplots with the largest amount of variance amount of variance support the fact that the d eposition process is non-uniform, which also shown in Figures 11 and 12 where compositional segregation occur. The lowest average readings with low variance occurred at the pure Nb side, which was expected from Nb being a soft metal. The measurements taken were also based on distance along the gradient, therefore estimating the composition associated with the hardness measurements taken.

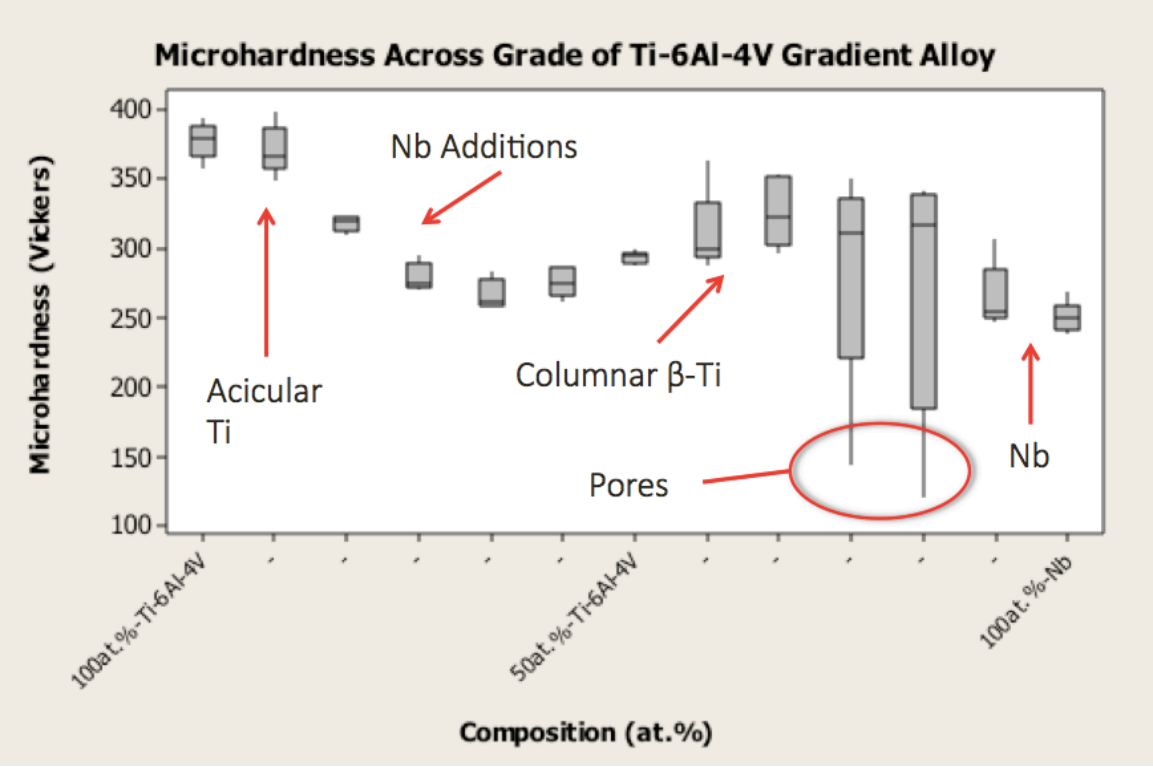

Figure 17: Hardness measurements in Vickers, with key microstructural features highlighted on graph.

Conclusions

The results of this study show that an annealed Ti structure does not form at any point along the gradient. The diffusion occurring in the melt pool of a Ti-6Al-4V to Nb gradient is also reflected in the scan enough to be considered as a non-negligible factor. Microstructures further support that diffusion, although slight, is significant at key points such as 4 at.% Nb and 30 at.% Nb, where thicker β-Ti forms and columnar β-Ti contribute to a non-uniform deposition. This is contrary to what was suggested in the research done by JPL, which suggested that the residence time of the laser makes mass transport negligible during laser deposition. After 30 at.% Nb, α-Ti cannot be observed in the microstructure. With increasing Nb content, the amount of porosity within layers increased until 100 at.% Nb, where the layers also did not completely bond. XRD scans also further indicate that slight diffusion affects the structure significantly. Secondary HCP peaks disappear after 30 at.% and the main HCP peak becomes negligible after 55-60 at.%. Compositional data shows that the deposition of the gradient is increasing as expected, but reaching 100 at.% Nb in a shorter distance due to overmelting of the layers. Hardness data concludes that the addition of Nb generally decreases the hardness of the structure, where the variance of hardness measurements increases with pore-dense areas.

For Future Study

In order to close the pores of the microstructure, the incremental increases of laser power should be larger appropriate for the amount of Nb in a specific layer. Hot isostatic pressing should also be done in conjunction with a remodeling of the parameters for deposition. This should be done to achieve a microstructure that is more laterally uniform and closer to an annealed structure. To study the phases present in the structure and the orientations of each phase, an electron backscatter diffraction function (EBSD) on a scanning electron microscope should be used.

Appendix A: Run Log for Ti-6Al-4V to Nb Gradient Alloy

Ti-6Al-4V to Niobium		NOTES							
start layer	end layer	# layers	% volume Ti-6Al-4V	gpm Ti-6Al-4V	RPM Ti-6Al-4V	% volume Niobium	gpm Niobium	RPM Niobium	Watts
0	19	20	100.000%	6.605	5.022	0.000%	0.000	0.000	910
20	20	1	96.000%	6.341	4.820	4.000%	0.513	0.543	919
21	21	1	92.000%	6.077	4.618	8.000%	1.026	1.044	928
22	22	1	88.000%	5.813	4.416	12.000%	1.539	1.544	937
23	23	1	84.000%	5.548	4.214	16.000%	2.052	2.045	946
24	24	1	80.000%	5.284	4.011	20.000%	2.565	2.546	955
25	25	1	76.000%	5.020	3.809	24.000%	3.077	3.046	964
26	26	1	72.000%	4.756	3.607	28.000%	3.590	3.547	973
27	27	1	68.000%	4.491	3.405	32.000%	4.103	4.047	982
28	28	1	64.000%	4.227	3.203	36.000%	4.616	4.548	991
29	29	1	60.000%	3.963	3.001	40.000%	5.129	5.049	1000
30	30	1	56.000%	3.699	2.799	44.000%	5.642	5.549	1009
31	31	1	52.000%	3.435	2.597	48.000%	6.155	6.050	1018
32	32	1	48.000%	3.170	2.395	52.000%	6.668	6.550	1027
33	33	1	44.000%	2.906	2.193	56.000%	7.181	7.051	1036
34	34	1	40.000%	2.642	1.991	60.000%	7.694	7.551	1045
35	35	1	36.000%	2.378	1.789	64.000%	8.206	8.052	1054
36	36	1	32.000%	2.114	1.587	68.000%	8.719	8.553	1063
37	37	1	28.000%	1.849	1.385	72.000%	9.232	9.053	1072
38	38	1	24.000%	1.585	1.183	76.000%	9.745	9.554	1081
39	39	1	20.000%	1.321	0.981	80.000%	10.258	10.054	1090
40	40	1	16.000%	1.057	0.779	84.000%	10.771	10.555	1099
41	41	1	12.000%	0.793	0.577	88.000%	11.284	11.056	1108
42	42	1	8.000%	0.528	0.375	92.000%	11.797	11.556	1117
43	43	1	4.000%	0.264	0.172	96.000%	12.310	12.057	1126
44	62	19	0.000%	0.000	0.000	100.000%	12.823	12.557	1135

Appendix B: Microstructures with Increasing at.% Nb without Columnar β-Ti Formation

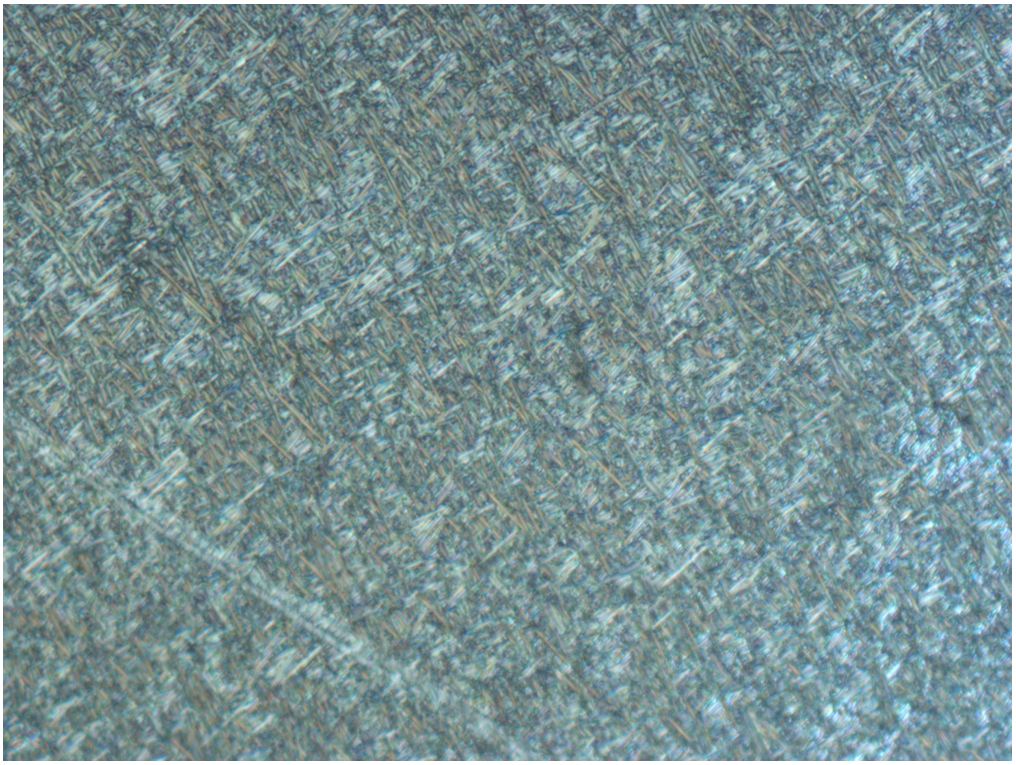

Figure B-1: Deposited layer at approximately 88 at.% Ti-6Al-4V, and 12 at.% Nb.

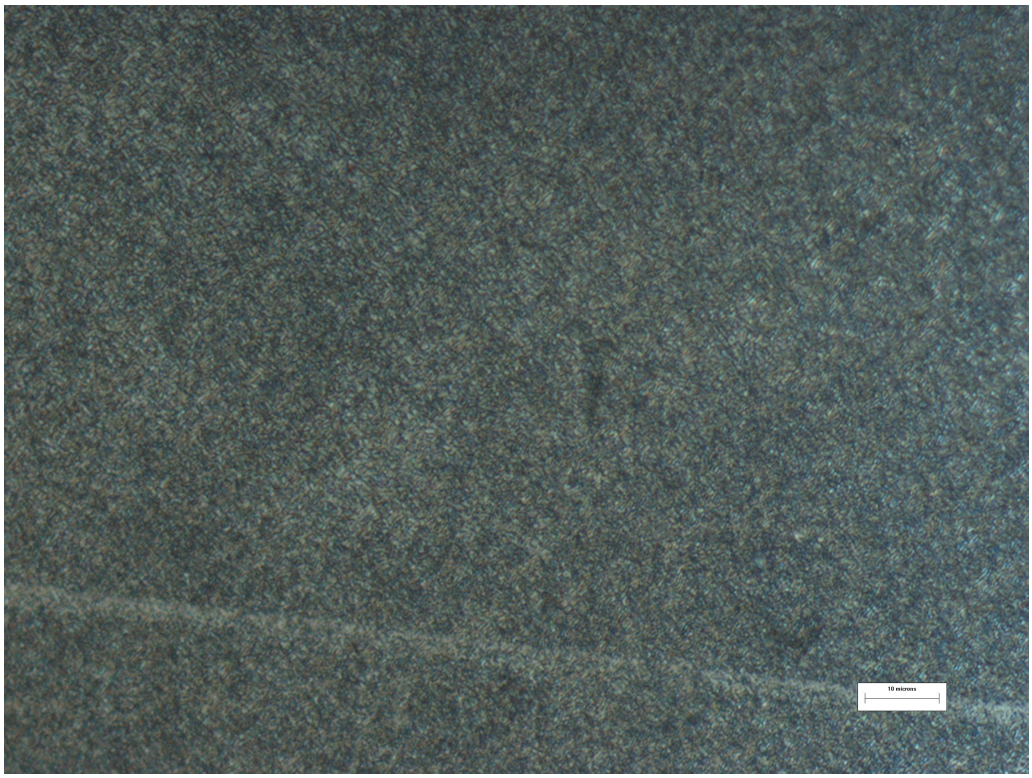

Figure B-2: Deposited layer at approximately 88 at.% Ti-6Al-4V, and 12 at.% Nb.

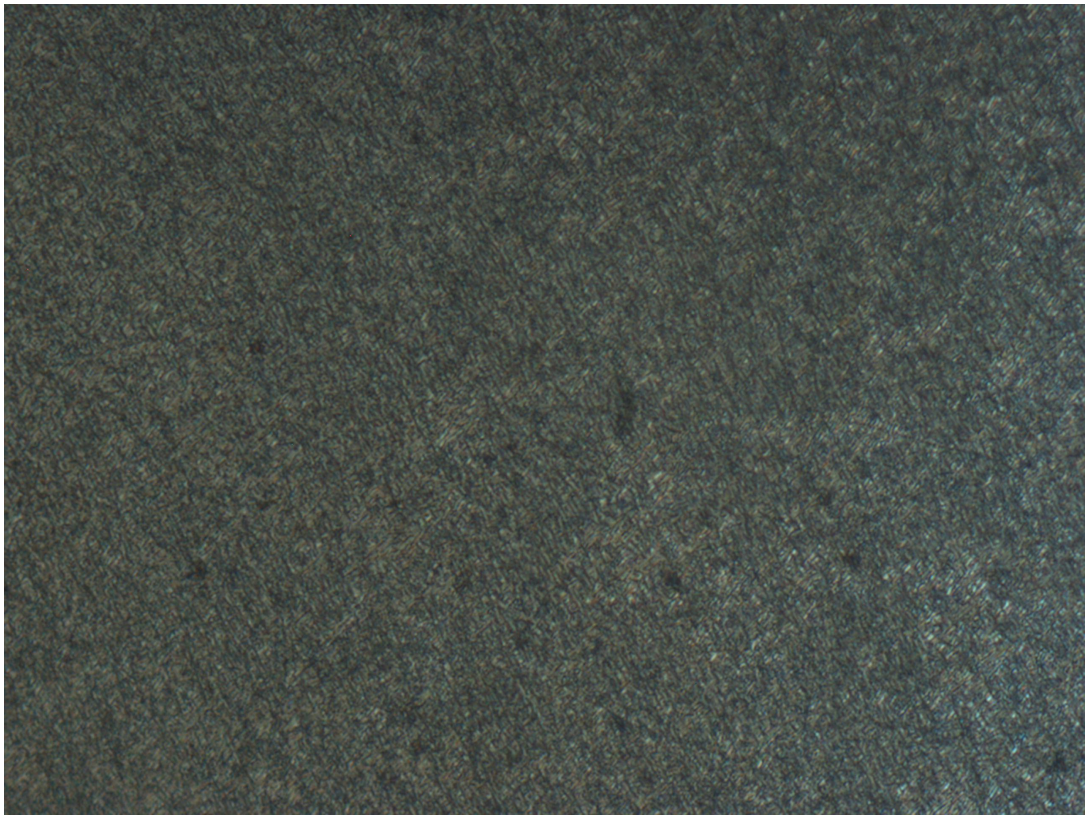

Figure B-3: Deposited layer at approximately 84 at.% Ti-6Al-4V, and 16 at.% Nb.

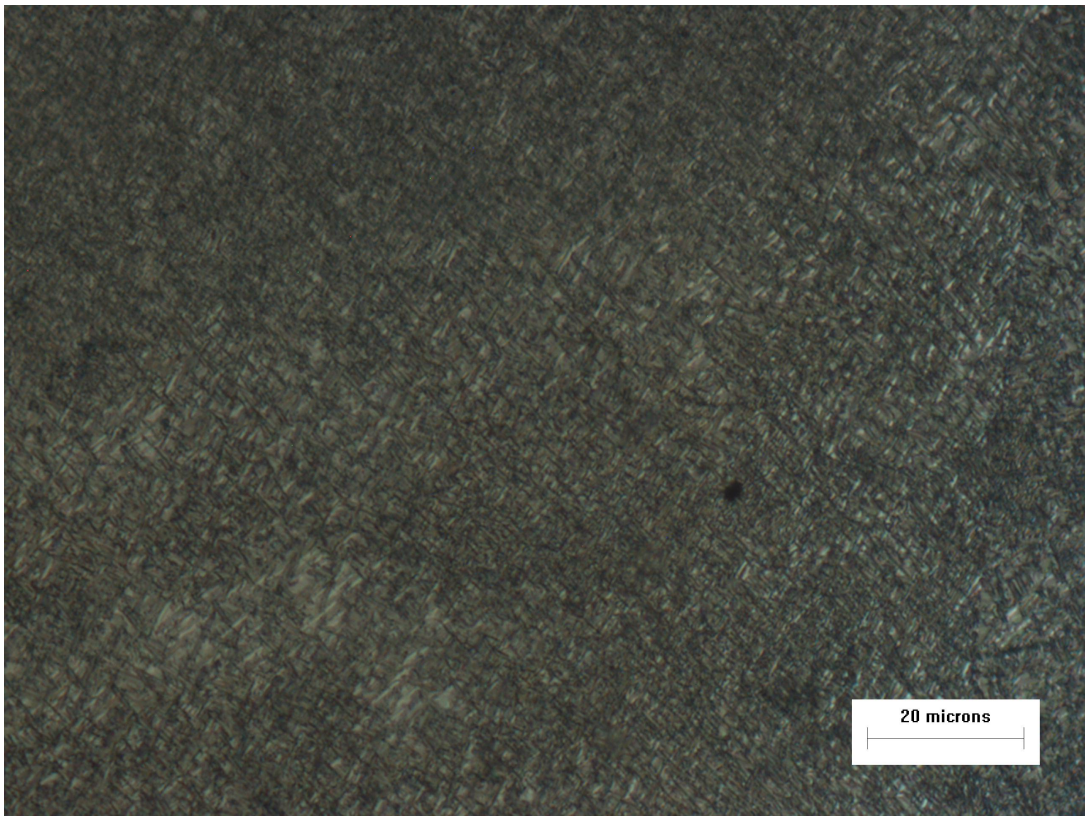

Figure B-4: Deposited layer at approximately 80 at.% Ti-6Al-4V, and 20 at.% Nb.

Appendix C: Raw XRD Scans, Overlay and 3-D Non-Interpolated Plot of Raw Scans

100 at.% Laser Deposited Ti-6Al-4V

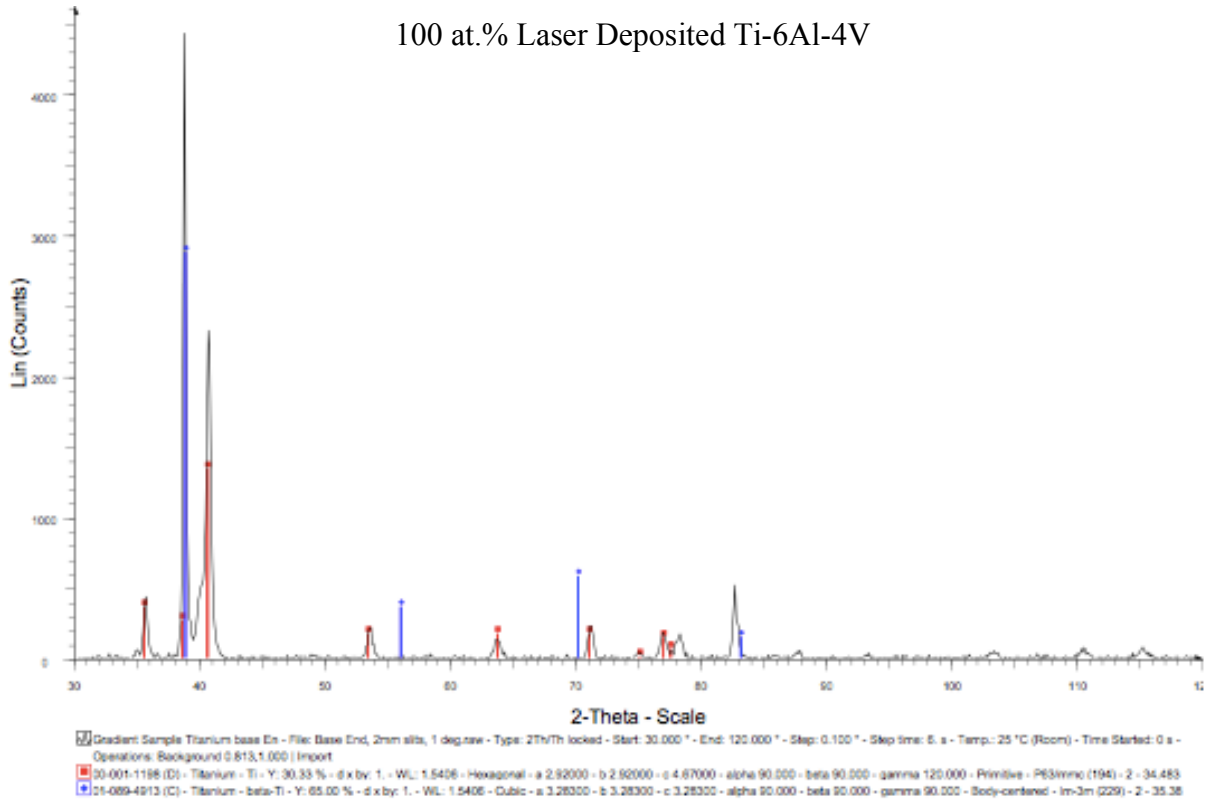

Forged Ti-6Al-4V Substrate

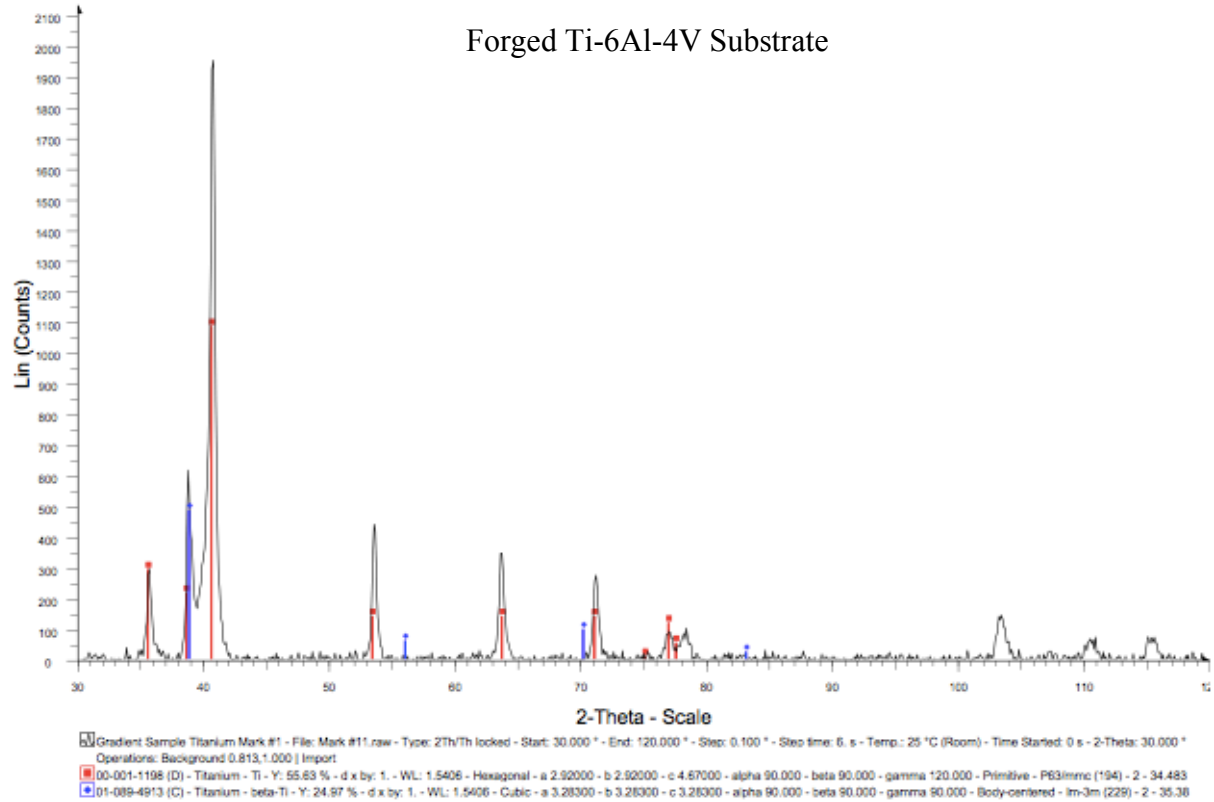

100 at.% Laser Deposited Nb

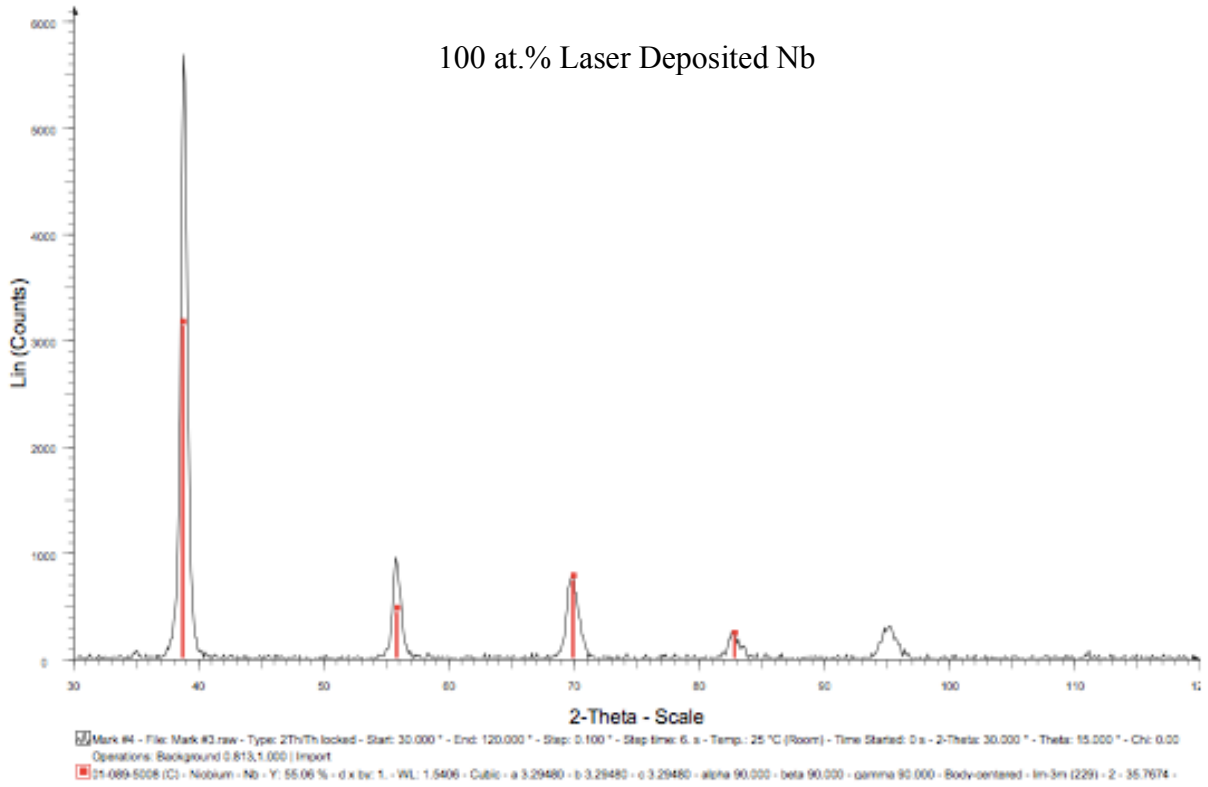

Overlay of All Scans

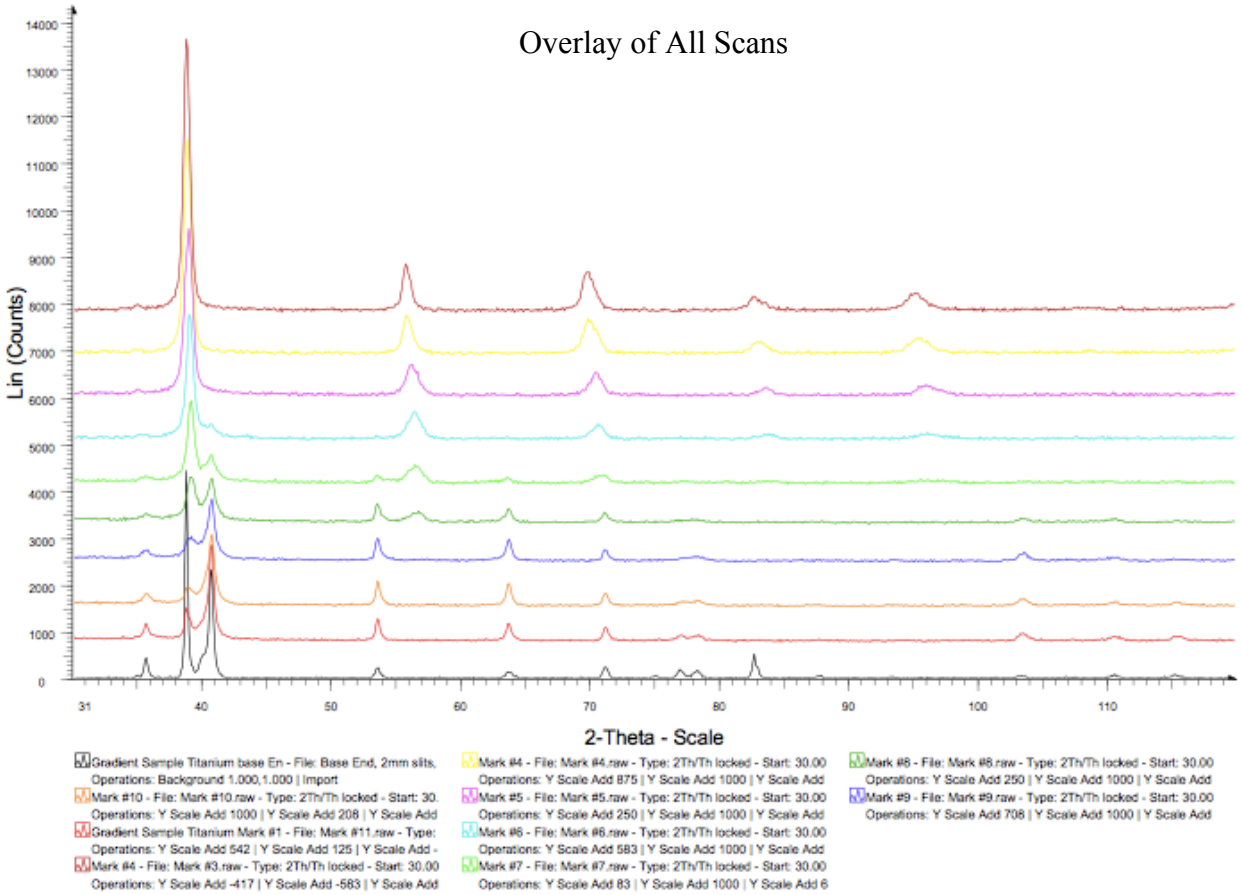

Appendix D: Raw Microhardness Measurements and Calculations

Layer	Measurement (Diag)	HV.
1	22.2	376.1869978
	21.7	393.7225254
	22.1	379.5991073
	22	383.0578512
	22.8	356.6481994
2	22.5	366.2222222
	21.6	397.3765432
	22.2	376.1869978
	22.5	366.2222222
	23.05	348.9537505
3	24	321.875
	24.2	316.5767366
	24.5	308.8713036
	24	321.875
	24.1	319.20938
4	26.2	270.0891556
	26	274.260355
	25.1	294.2810432
	25.5	285.1211073
	26	274.260355
5	26.8	258.1309869
	26.1	272.1627692
	26.6	262.0272486
	25.6	282.8979492
	26.7	260.0681732
6	25.45	286.2425265
	26.6	262.0272486
	26.2	270.0891556
	26	274.260355
	25.5	285.1211073
7	25.1	294.2810432
	25.4	287.3705747
	25.2	291.9501134
	24.9	299.027435
	25.1	294.2810432

Layer	Measurement (Diag)	HV.
8	24.9	299.027435
	24.8	301.4438085
	22.6	362.9884877
	25.4	287.3705747
	24.9	299.027435
9	23	350.4725898
	22.9	353.540169
	24	321.875
	24.5	308.8713036
	25	296.64
10	35.9	143.8536324
	24.05	320.5380336
	23	350.4725898
	24.9	299.027435
	24.4	311.4082236
11	27.3	248.7622268
	39.3	120.0396247
	24.2	316.5767366
	23.5	335.7175192
	23.3	341.5056457
12	27.1	252.4475429
	26.6	262.0272486
	24.6	306.3652588
	27	254.3209877
	27.4	246.9497576
13	27.2	250.5947232
	27.6	243.3837429
	27.9	238.177824
	27.2	250.5947232
	26.3	268.0391505

Appendix E: Raw EDS Results

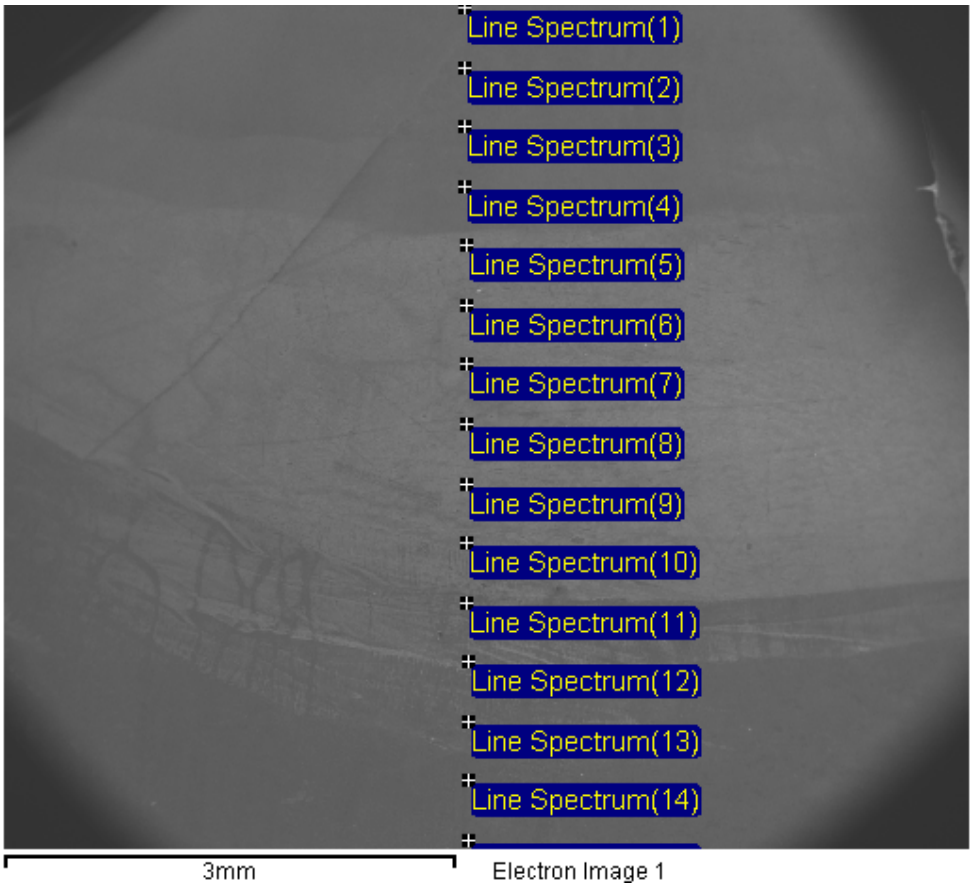

Spectrum	In stats.	Al	Ti	V	Nb	Total
Line Spectrum(1)	Yes	5.24	90.58	4.18		100.00
Line Spectrum(2)	Yes	4.91	90.56	4.53		100.00
Line Spectrum(3)	Yes	5.08	90.40	4.52		100.00
Line Spectrum(4)	Yes	4.89	86.46	4.36	4.30	100.00
Line Spectrum(5)	Yes	4.57	83.71	4.29	7.42	100.00
Line Spectrum(6)	Yes	4.64	81.43	4.27	9.67	100.00
Line Spectrum(7)	Yes	4.57	81.93	4.35	9.15	100.00
Line Spectrum(8)	Yes	3.61	72.93	4.65	18.81	100.00
Line Spectrum(9)	Yes	3.56	69.56	4.23	22.65	100.00
Line Spectrum(10)	Yes	3.58	67.41	3.63	25.38	100.00
Line Spectrum(11)	Yes	3.62	65.70	3.52	27.16	100.00
Line Spectrum(12)	Yes	3.39	66.32	3.43	26.86	100.00
Line Spectrum(13)	Yes	3.40	61.14	3.11	32.35	100.00
Line Spectrum(14)	Yes	2.95	55.83	2.83	38.38	100.00
Line Spectrum(15)	Yes	2.97	52.70	2.87	41.47	100.00
Max.		5.24	90.58	4.65	41.47	
Min.		2.95	52.70	2.83	4.30	

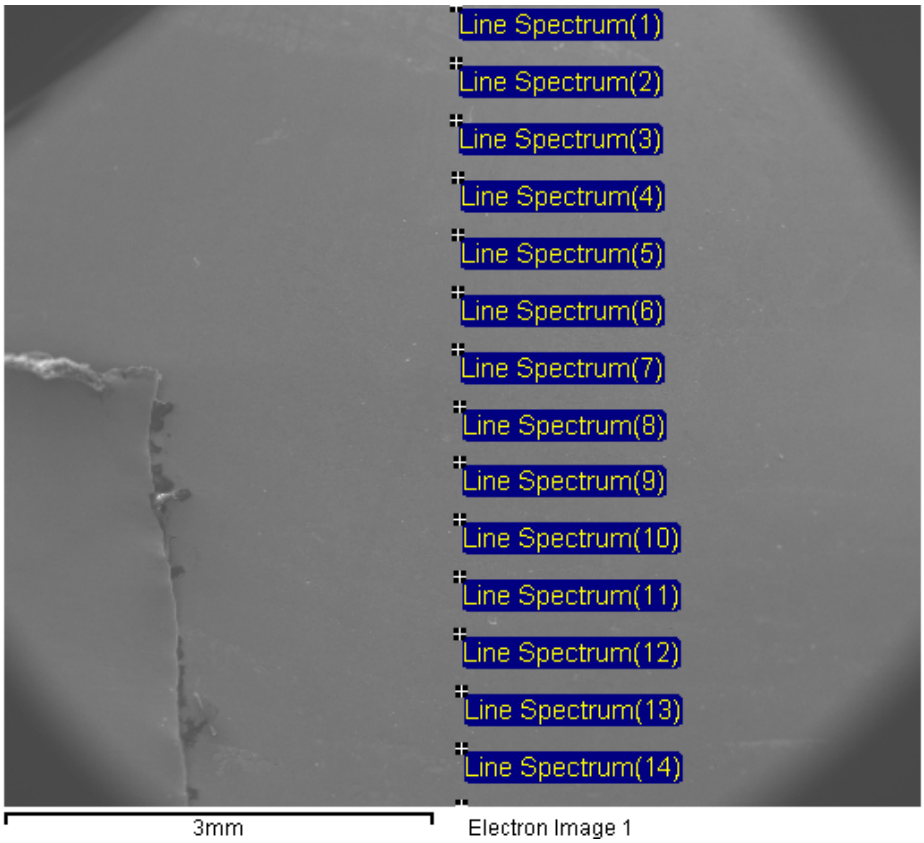

Spectrum	In stats.	Al	Ti	V	Nb	Total
Line Spectrum(1)	Yes	3.57	62.04	3.23	31.16	100.00
Line Spectrum(2)	Yes	3.55	61.38	2.99	32.08	100.00
Line Spectrum(3)	Yes	3.25	55.66	2.83	38.26	100.00
Line Spectrum(4)	Yes	3.00	51.63	2.46	42.91	100.00
Line Spectrum(5)	Yes	2.96	50.55	2.60	43.89	100.00
Line Spectrum(6)	Yes	2.67	46.40	2.39	48.54	100.00
Line Spectrum(7)	Yes	2.57	44.50	2.35	50.58	100.00
Line Spectrum(8)	Yes	2.29	40.73	2.25	54.74	100.00
Line Spectrum(9)	Yes	2.03	33.47	1.61	62.89	100.00
Line Spectrum(10)	Yes	1.52	27.26	1.31	69.92	100.00
Line Spectrum(11)	Yes	1.63	29.95	1.76	66.66	100.00
Line Spectrum(12)	Yes	1.36	24.84	1.41	72.40	100.00
Line Spectrum(13)	Yes	0.82	17.71	1.03	80.44	100.00
Line Spectrum(14)	Yes	1.22	19.72	1.06	77.99	100.00
Line Spectrum(15)	Yes	0.64	13.22	0.64	85.49	100.00
Mean		2.20	38.60	1.99	57.20	100.00
Std. deviation		0.97	16.10	0.79	17.85	
Max.		3.57	62.04	3.23	85.49	
Min.		0.64	13.22	0.64	31.16	

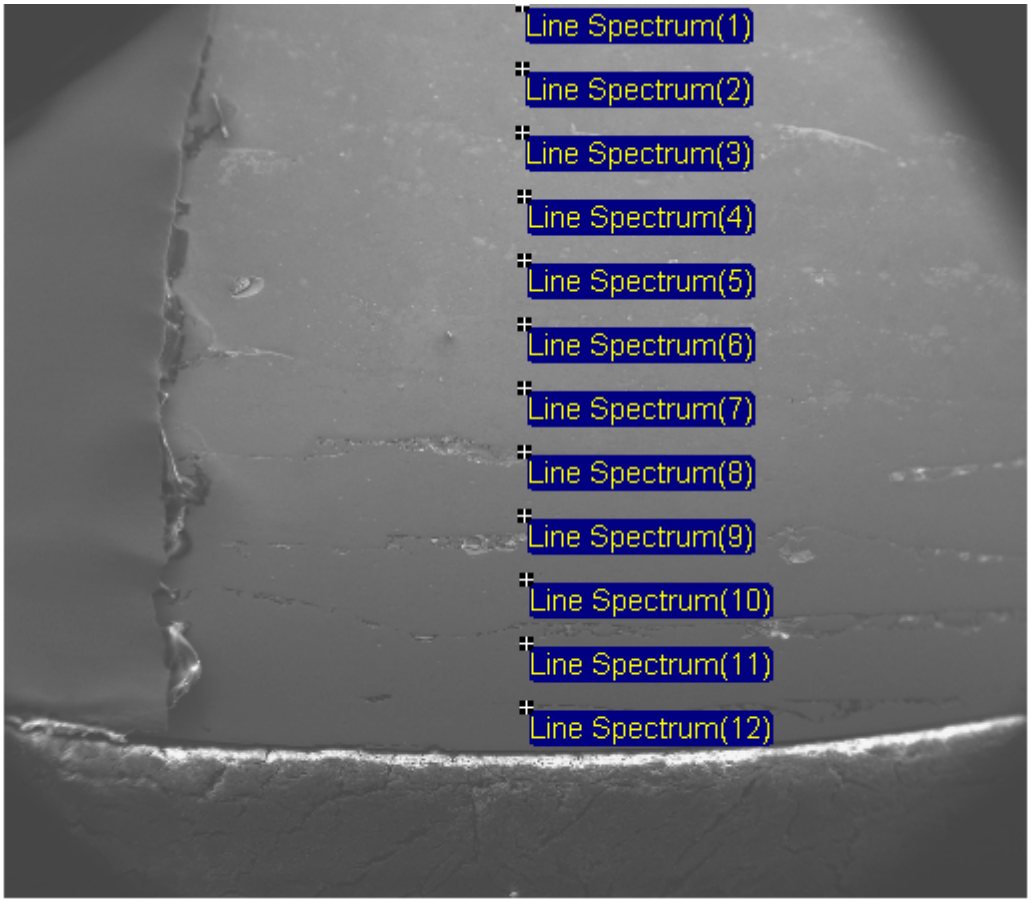

Spectrum	In stats.	Al	Ti	V	Nb	Total
Line Spectrum(1)	Yes	1.36	22.93	1.07	74.65	100.00
Line Spectrum(2)	Yes	0.95	17.57	0.77	80.72	100.00
Line Spectrum(3)	Yes	1.05	18.03	0.90	80.01	100.00
Line Spectrum(4)	Yes	0.81	12.95	0.74	85.50	100.00
Line Spectrum(5)	Yes	0.68	10.69	0.73	87.90	100.00
Line Spectrum(6)	Yes		6.00		94.00	100.00
Line Spectrum(7)	Yes				100.00	100.00
Line Spectrum(8)	Yes		0.49		99.51	100.00
Line Spectrum(9)	Yes				100.00	100.00
Line Spectrum(10)	Yes				100.00	100.00
Line Spectrum(11)	Yes				100.00	100.00
Line Spectrum(12)	Yes				100.00	100.00
Max.		1.36	22.93	1.07	100.00	
Min.		0.68	0.49	0.73	74.65	

References

1. Hofmann, Douglas C., Scott Roberts, Richard Otis, Joanna Kolodziejska, R. Peter Dillon, Jong-Ook Suh, Andrew A. Shapiro, Zi-Kui Liu, and John-Paul Borgonia. "Developing Gradient Metal Alloys through Radial Deposition Additive Manufacturing." *Scientific Reports Sci. Rep.* 4 (2014): n. pag. Web.

2. Erinosho, Mutiu F., Esther T. Akinlabi, and Sisa Pityana. "Laser Metal Deposition of Ti6Al4V/Cu Composite: A Study of the Effect of Laser Power on the Evolving Properties." *Proceedings of the World Congress on Engineering* 2 (2014): 1205-206. *IAENG*. Web. <http://www.iaeng.org/publication/WCE2014/WCE2014_pp1202-1207.pdf>.

3. Liu, C.m., X.j. Tian, H.b. Tang, and H.m. Wang. "Microstructural Characterization of Laser Melting Deposited Ti–5Al-5Mo–5V–1Cr–1Fe near β Titanium Alloy." *Journal of Alloys and Compounds* 572 (2013): 450-51. Web.

4. F., Vander Voort George. *Metallography, Principles and Practice*. Materials Park, OH: ASM International, 1999. Print.

5. ASTM E384: "Test Method for Microindentation Hardness of Materials." ASTM International. 2010. Web.

6. Pederson, Robert. "Microstructure and Phase Transformation of Ti-6Al-4V." *Lulea University of Technology* (2002): 10-13. Web. <http://epubl.luth.se/1402-1757/2002/30/LTU-LIC-0230-SE.pdf>.

7. Donachie, Matthew J. "Chapter 9: Joining Technology and Practice." *Titanium: A Technical Guide (2nd)*. Metals Park, OH: ASM International, 2000. 67. Print.

8. Nb (Niobium) Binary Alloy Phase Diagrams, *Alloy Phase Diagrams*, Vol 3, *ASM Handbook*, ASM International, 1992, p 2.304–2.308.